ADVANCED ENERGY MATERIALS
www.advenergymat.de

Solid-State Solar Thermal Fuels for Heat Release Applications

*David Zhitomirsky, Eugene Cho, and Jeffrey C. Grossman**

Closed cycle systems offer an opportunity for solar energy harvesting and storage all within the same material. Photon energy is stored within the chemical conformations of molecules and is retrieved by a triggered release in the form of heat. Until now, such solar thermal fuels (STFs) have been largely unavailable in the solid-state, which would enable them to be utilized for a multitude of applications. A polymer STF storage platform is synthesized employing STFs in the solid-state. This approach enables uniform films capable of appreciable heat storage of up to 30 Wh kg^{-1} and that can withstand temperature of up to 180 °C. For the first time a macroscopic energy release is demonstrated using spatial infrared heat maps with up to a 10 °C temperature change. These findings pave the way for developing highly efficient and high energy density STFs for applications in the solid-state.

1. Introduction

Solar energy is an abundant yet underexploited energy resource on Earth. Though several large-scale solar energy harvesting and storage solutions have been developed (such as large-area solar cells), there is tremendous opportunity for smaller scale device applications for industrial and consumer use. Closed cycle systems,[1,2] such as ones employing cyclable energy storage within the bonds of organic chromophores, offer the unique advantage of energy harvesting and storage all within the same material. Furthermore, in some applications, heat rather than electrical energy may be required, where these materials have their greatest potential.

The practical aspects of a solar thermal fuel (STF) involve absorbing photons of energy sufficient to cause an electronic transition that then drives an isomerization or reversible chemical process. The isomerized, higher energy, state of a practical STF stores a substantial portion of this photon energy and has the necessary energetics to prevent substantial thermal reversion at storage conditions. Solution-state STFs have been explored as large-scale energy storage materials given the norbornadiene/quadricyclane system and its high energy density (≈280 Wh kg^{-1}).[3,4] However, these materials were soon abandoned due to low cyclability, limiting long-term use. In other approaches, new materials with modest energy storage (56 Wh kg^{-1}) employing ruthenium with higher cyclability have been developed,[5–7] but remain prohibitively expensive for wide adoption. With the availability of accurate computational tools, new approaches have leveraged carbon nanostructures and insights into the steric interaction of STFs to increase energy density employing highly cyclable and modest energy density (60–70 Wh kg^{-1}) azobenzene derivatives.[8,9] While demonstrating a per-molecule increase in energy density via templating,[10] these approaches require complex multistep reactions, have low yields, and the resulting material has low solubility in most organic solvents (<1 g L^{-1}). More recently, it was possible to develop liquid azobenzene fuels at room temperature by attaching bulky ligands to the molecule,[11] and with several computational works detailing the possibility of increasing its energy density through functionalization of the benzene rings,[12] this platform holds much promise for future STF developments. With such rapid progress in STF materials, it is perhaps surprising that the solid-state platform and related applications have remained largely unexplored, with only recent studies on semi-solid photoliquefiable ionic crystals reaching energy densities of 35 Wh kg^{-1}.[13] Transitioning fully to the solid-state offers the possibility of integrating STF materials into a multitude of existing solid-state devices such as coatings for deicing, or novel applications such as solar blankets and other consumer oriented heating equipment.

We took the view that if properly engineered on the molecular level, STF materials could be controllably tailored within the solid-state, and that until now, there has not been an efficient method to accomplish this. For one, the most recent STF reports have relied on carbon scaffolds[10,14] that simultaneously increase synthesis complexity, cannot be deposited into uniform films, contribute to the optical density without resulting in photocharging, and introduce uncontrollable morphological effects that may limit charging and reversible switching in the solid-state.[15] Similarly, single-molecule thin films do not make homogenous layers, can often result in crystallization, and melt at low temperatures (≈70 °C for azobenzene) thus limiting their utility in the solid-state. Fortunately, a wealth of literature exists on azobenzene-based materials in solid-state applications for microswitches, microactuators, and sensors.[16–21] We postulated that the ideal material class to form solid-state STF coatings would need to (1) form smooth films with controllable thickness, (2) be resilient at high temperatures, (3) preserve the heat release properties of

Dr. D. Zhitomirsky, E. Cho, Prof. J. C. Grossman
Department of Materials Science and Engineering
Massachusetts Institute of Technology
Cambridge, MA 02139, USA
E-mail: jcg@mit.edu

DOI: 10.1002/aenm.201502006

the molecular STF counterparts and maximize the energy density, (4) enable charging, storage, and discharging on device-relevant timescales, and (5) exhibit feasibility for large area heat release applications. In this regard, we chose to develop a polymer solid-state platform that, if engineered correctly, would be sufficiently tunable and scalable to satisfy these requirements. Importantly, the rich chemistry available on both the monomer and polymer backbone enables the application of the same computational design principles previously employed for single molecule STFs,[12] while also revealing a newly accessible engineering space given polymer–polymer chain interaction, cross-linking degree, and conjugation within the polymer backbone.

2. Results and Discussion

While several reports have employed azobenzenes as part of the polymer backbone,[22,23] we instead opted for an approach with more conformational freedom where azobenzene moieties comprised the polymer side chains while simultaneously maximizing the azobenzene density in the form of homopolymers.[24–26] **Figure 1**a depicts such a polymer, where the backbone is comprised of an alkyl chain while the side chains are made up of azobenzenes. When illuminated with photons of an appropriate energy, the low energy *trans*-azobenzene molecules would ideally change their conformation to the *cis*-state, despite any steric effects resulting from neighboring side-chain interactions.

Our chosen monomer along with a synthetic route is shown in Figure 1b, where an acrylate group is attached to an azobenzene derivative to enable polymerization with common radical initiators. Given that adding new functional groups can drastically change the energetic[12] and optical[27] properties of azobenzenes, we first verified our intended monomer via density functional theory (DFT). DFT simulations revealed a modest potential energy density of 68 Wh kg^{-1} for the monomer species, indicating the additional substituent had not caused a major change in the expected energy density compared to azobenzene (76 Wh kg^{-1} from DFT).

Size exclusion chromatography (SEC) on the synthesized polymer (Figure 1c) enabled us to estimate an average of 45 monomer units per polymer chain (referenced to polystyrene), and reproducibly scale to the gram scale with an overall reaction yield of ≈60%. Despite a high probability for steric hindrance during synthesis, these polymers grow to sufficiently large sizes and are capable of being dissolved in organic solvents compatible with spin coating in order to make solid-state thin films. Additionally, generating these materials in a facile two-step chemical process presents an attractive avenue toward scalability and inexpensive production.[28]

The key aspect of effective materials design relies in leveraging the excellent properties of certain small molecule STFs and transitioning them into the solid-state in the form of polymers. In this respect, it is important to compare the monomer and polymer moieties to ensure retention of STF properties. Absorption spectra (**Figure 2**a) revealed consistent optical properties between the two materials, with a slight

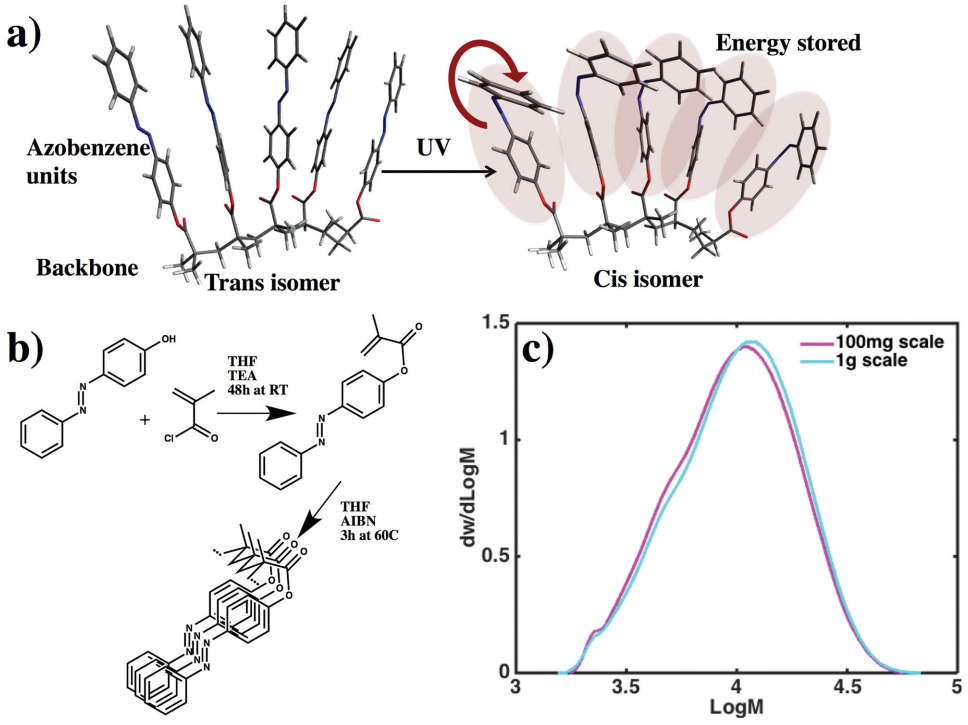

Figure 1. Solid-state solar thermal fuel polymer concept. a) A schematic of an azobenzene polymer consisting of four monomers in the *trans*-state being converted to the *cis*-state upon UV illumination. The result is the apparent rotation of that azobenzenes about the N=N double bond. b) Chemical synthesis scheme for generating the homopolymer by employing a radical polymerization of an azobenzene monomer. c) Size exclusion chromatography performed to analyze polymer samples and deduce the distribution, as well as reproducibility with a scaled-up synthesis.

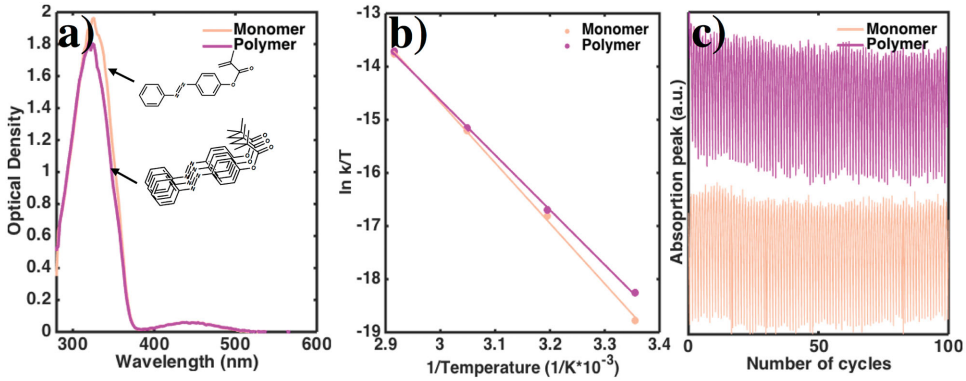

Figure 2. Monomer and polymer properties. a) Solution absorption spectra of the monomer and polymer exhibiting two prominent peaks, where the high-energy peak at 325 nm corresponds to the $\pi > \pi^*$ transition enabling *trans* to *cis* isomerization. b) Eyring–Polanyi plots used to extract the reverse thermal isomerization barrier energy associated with the discharge process. c) Cycling plots demonstrating the long-term cyclability of the two species to ascertain the feasibility for long-term material use.

reduction in absorption in the polymer. Similar to azobenzene, the *trans*-dominant peak exists in the UV at 325 nm, while the *cis*-state develops an optically accessible peak at 450 nm. As has been extensively reported for azobenzene,[29] exciting these materials via the $\pi > \pi^*$ transition results in the reduction of the high-energy peak and emergence of the low-energy peak. The magnitudes of these peaks play a crucial role in the extent to which solid-state films of the polymer may be charged. In Figure 2b, an Eyring–Polanyi plot (Section S1, Supporting Information) enables to extract the reverse isomerization energy barrier often denoted as Ea, for the monomer (95 ± 2 kJ mol^{-1}) and polymer (86 ± 2 kJ mol^{-1}). Azobenzene derivatives may be engineered to have a *cis*-state lifetime spanning several microseconds to days by tailoring the functional groups attached to the phenyl rings.[30,31] Our materials exhibit room temperature (25 °C) half-lives (time taken for 50% of the *cis* isomer to decay back to *trans*) of 92 ± 1 and 55 ± 1 h for the monomer and polymer species, respectively (Section S1, Supporting Information), suitable for energy storage in applications requiring daily cycles. Finally, in order to be suitable for long-term use, the cyclability of these materials was tested in Figure 2c, where photon sources were used to cycle the materials between the *trans*- and *cis*-states; retention of the optical and thus material properties was maintained for over 100 cycles.

In order to transition the materials to the solid-state, several facile strategies are available, such as tape-casting, drop-casting, and spin-coating. The former two techniques generally result in morphologically poor films, however enable high thicknesses, while the latter results in good morphology but at the cost of low thickness or incomplete coverage at low spin speeds. **Figure 3**a depicts the development of our solid-state STF platform by constructing a simple solar thermal energy capacitor (STEC) using a transparent fixed-size 1 in. quartz substrate and depositing the STF materials on top using toluene via spin-coating. Such a device ensures that it is possible to monitor the optical properties during charging and discharging cycles, and allows for highly reproducible samples. Upon inspection of optical microscope images comparing the monomer and polymer STECs in Figure 3b,c, it is immediately evident that the polymer approach is ideal for the development of smooth and crack-free films. Cross-sectional analysis (Figure 3d) revealed that the polymer films are highly uniform in thickness.

In order to see the scalability of the spin-coating process, we experiment with solution concentrations spanning 25–100 mg mL^{-1}, where the latter regime approaches the solubility limit of the material in toluene. Figure 3e shows that using the 50 mg mL^{-1} process, more than 99% of the light is absorbed, while the 100 mg mL^{-1} process saturates the detector. In Figure 3f,g, the mass and thickness of the STF film is plotted for each type of STEC process (in this case, concentration variation). Importantly, a film of 1 µm has a mass in the range of several milligrams and can already absorb all of the light in the UV region. This result, along with the energy density of the material, is crucial in determining the thickness and charging requirements for the material because while at greater thicknesses and masses the total energy is increased, the photon penetration depth and thus charging is highly stagnated given some nonunity photostationary *cis*-state.[32]

Differential scanning calorimetry (DSC) measurements were used to accurately determine the energy storage potential of our STF materials. **Figure 4**a shows heat release curves for the monomer (42 ± 2 Wh kg^{-1}) and polymer (29 ± 2 Wh kg^{-1}) moieties charged in solution (toluene); importantly, no melting regime was observed for the polymer in this temperature range (Section S2, Supporting Information). Such a difference in energy density may arise from variation in photoswitching quantum yield, absorption, and thermal reversion barriers, influencing the photostationary state.[32] Steric hindrance may prevent photoswitching in the solid-state due to presence of both rotation (steric-sensitive) and inversion mechanisms for isomerization,[33,34] thus limiting the performance of the STECs. In order to test this, we illuminated our polymer STEC with UV (365 nm center mercury lamp) and recorded their absorption spectra. As shown in Figure 4b, the initial uncharged STEC transitions to a charged state upon irradiation, evident through a reduction in the 325 nm peak corresponding to the $\pi > \pi^*$ transition and emergence of the 450 nm peak (corresponding to the *cis* $n > \pi^*$ transition). Upon mild heating (80 °C), the initial spectrum is fully recovered, with more rigorous heat resilience tested at temperatures approaching 180 °C (Section S3, Supporting Information). Despite optical evidence of photoswitching, the exact

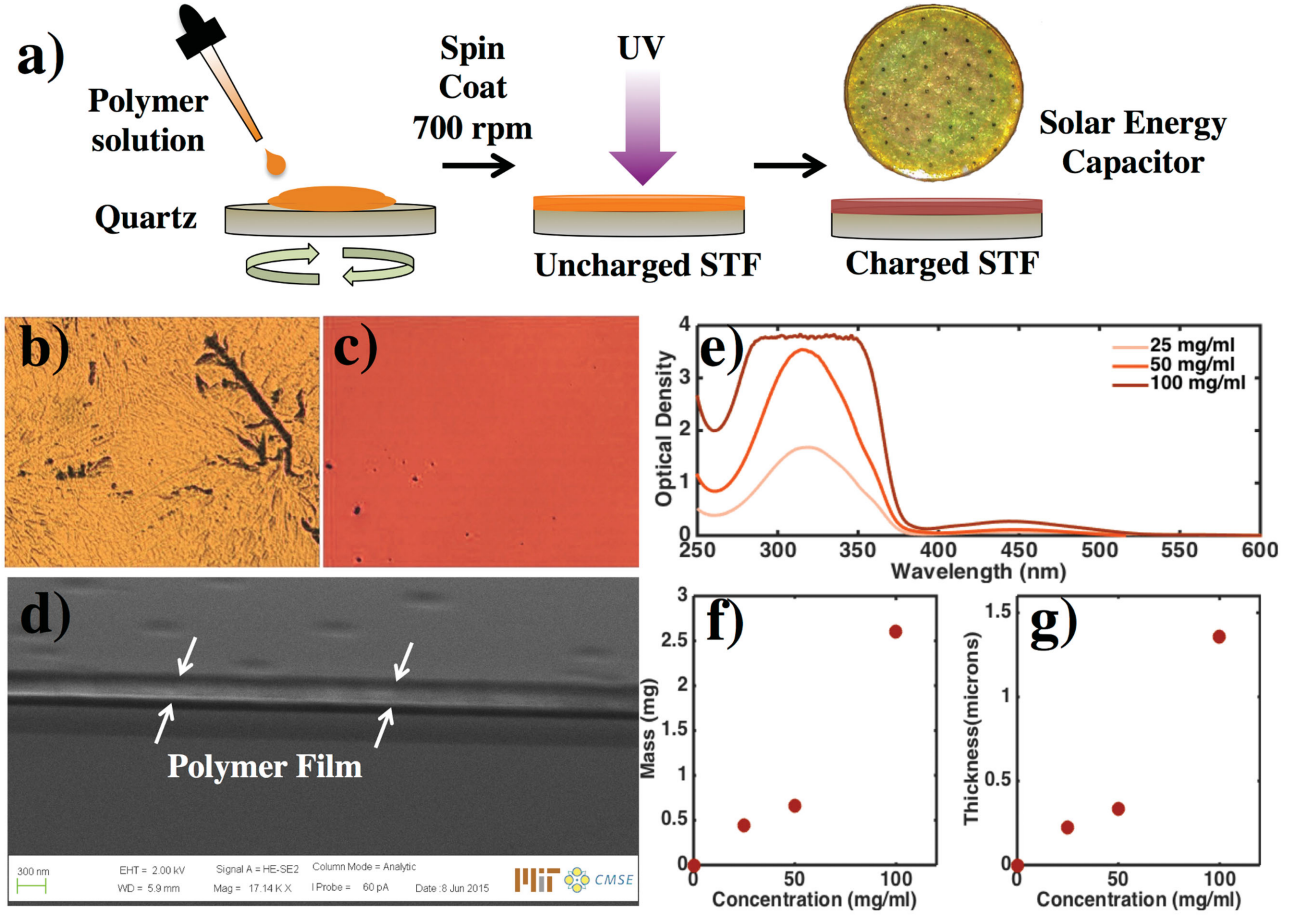

Figure 3. Solid-state polymer solar thermal fuel films. a) Schematic of the spin-coating process employing the polymer solution in toluene with a transparent quartz substrate. Charging is accomplished with UV illumination using a lamp centered at 365 nm. Inset shows a 1 in. diameter semi-transparent solar thermal energy capacitor atop a clean room matt. b,c) Color-adjusted optical microscope images of the monomer and polymer spin-coated films, respectively (2 mm *y*-axis). The polymer films are smooth compared to the highly rough monomer films. d) Cross-sectional SEM image of the polymer film atop silicon exhibiting uniform thickness. e) Solid-state absorption spectra obtained on several samples with variable processing conditions based on polymer STF concentration in solution. f,g) Polymer film mass and thickness, respectively, for the processing conditions in (e).

energy density of the STEC must be measured once it is charged in solid-state. In order to achieve this, an STEC (25 mg mL^{-1} process) was charged and redissolved and dried within a DSC pan. As shown in Figure 4a, a similar energy density was measured as in the solution-state, with an average energy density of 26 ± 1 Wh kg^{-1} based on five identical trials. Compared to conventional electrochemical storage methods, the energy density stored within our solid-state STF materials approaches the lead acid battery (30–50 Wh kg^{-1}) and is superior to supercapacitors (0.05–5 Wh kg^{-1}).[35] A summary of the heat release and storage properties of these materials is presented in **Table 1**.

To achieve a large heat release per unit area, the total energy stored within the material is most easily increased with thickness, but at the cost of light penetration. As the material is charged, it consists of an advancing front of newly converted *cis* isomer (weakly absorbing UV) followed by the uncharged *trans* portion; however, due to a nonunity photostationary state in these systems, and nonzero absorption by the *cis* isomer in the spectral region of our UV lamp, the UV penetration will be stagnated thus greatly increasing the charging time. Figure 4c shows STECs that have been charged and measured to within 90% of their fully charged state for two different processing conditions. The rise of the energy density as a function of time is very rapid at first but then stagnates. For the 100 mg mL^{-1} process (≈1–2 µm, 2–3 mg), the charging time is more than a day; however, charging still takes place despite over 99.9% of the light being absorbed within the first 400–500 nm in the uncharged film (Figure 3e,g). Similar to charging properties of the STEC, it is important to verify the discharging expectation when transitioning between solution and film. Figure 4d plots the relative fraction of remaining *cis* isomer after charging in both solution and solid-state. Fitting with an exponential decay, the solid-state material can achieve 20%–40% (best, plotted) improvement in the decay constant, extending the lifetime of the charged stage. This is consistent with crystalline-phase azobenzene small molecules having greatly increased thermal activation barriers for the *cis* isomer in the solid-state.[36] Importantly, such length-scales are sufficiently adequate for

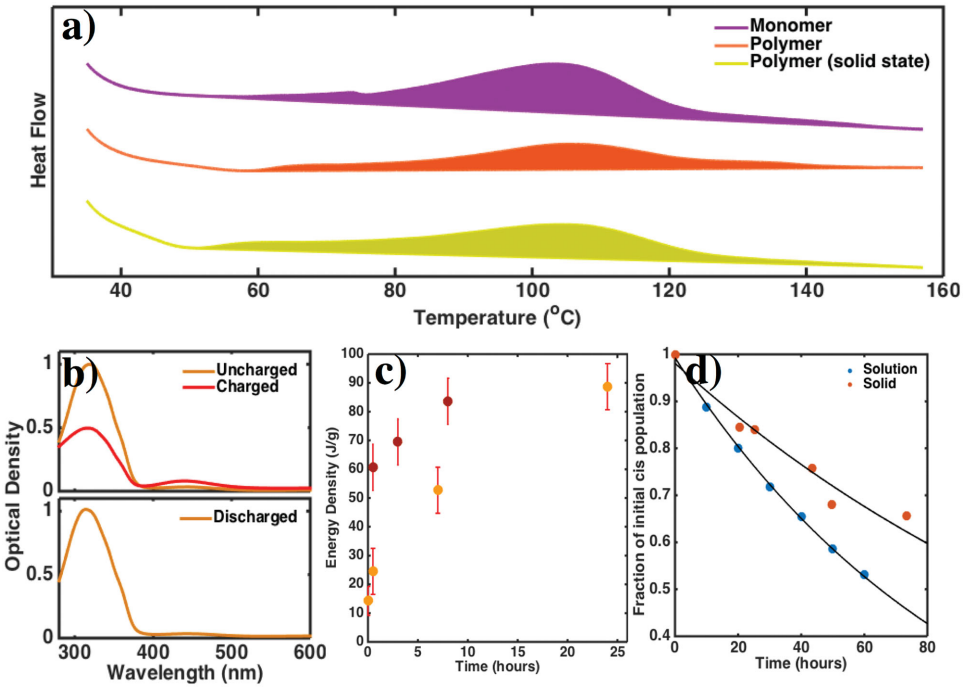

Figure 4. Charging, discharging, and thermal properties of solid-state polymer solar thermal fuels. a) Differential scanning calorimetry traces for monomer and polymer charged under various conditions. +γ direction represents heat release and the Gaussian regions colored overtop a flat baseline represent the integrated energy release. b) Photocharging of the polymer STF film visualized through absorption. Reduction of the high-energy 325 nm peak and increase in the 450 nm peak is indicative of the *trans* to *cis* transition. A single film is first charged (top) and then discharged (bottom) returning to its original state. c) Energy density measured on solar thermal energy capacitors charged in the solid-state as a function of time. With greater thickness the charging time is dramatically increased. d) Comparison of discharging the polymer STF samples in the dark between the solution and solid-state. The solid-state STF polymer has enhanced lifetime for the *cis*-state.

daily solid-state applications where energy may be stored effectively for later use.

In order to meet the requirements of a tunable solid-state STF platform, the STEC must have thickness (and thus mass) control well into the micrometer and millimeter scales. Ideally, the spin-coating process could be extended to make multiple layers by repeated deposition cycles; however, we found that repeated exposure to more STF in a solvent simply redissolved the underlying film. To remedy this, we developed a hybrid scheme where a liquid cross-linking polymer (poly(ethylene glycol) diacrylate PGda, $n = 250$) was used to readily dissolve our STF polymer. The resultant solution is then spin coated and UV cured (**Figure 5**a) thereby generating an insoluble layer. The film thickness may be controllably increased in such a way, however, with the drawback of a reduction in the gravimetric energy density.

As an initial test of this approach, we were able to generate a thick (>1 mm), flexible, and freestanding polymer STF film (Figure 5b) by UV-crosslinking the liquid STF hybrid. This large-scale film was insoluble and showed incorporation of the STF given its orange color. Upon cross-linking, the PGda forms a rigid network that traps the STF polymer inside (Figure 5c). Given that the number of PGda units is tunable, such an approach can generate films with different steric properties that could in principle be designed to increase the energy density of the STF themselves.[37] Additionally, the cross-linker may be tailored to have absorption that overlaps strongly with the *cis* isomer, thus limiting the rate of back reaction and leading to a higher photostationary state. Absorption spectra on single layer films with and without cross-linker (Figure 5d) revealed that the cross-linking does not interfere with charging of the STF films, as evident by the reduction of the 325 nm peak after charging. Furthermore, the cross-linker does not limit absorption, given minimal absorption for a comparable thickness film in the spectral region required for the $\pi > \pi^*$ STF transition. However, the STF polymer may prevent cross-linking of PGda itself due to its strong absorption, hence UV crosslinking requires careful balancing of both species.

In order to demonstrate the formation of a layer-by-layer film, the polymer STF was mixed into the UV-crosslinker at a 1:10 STF to cross-linker unit ratio. Tailoring the spin speed enabled to form thin viscous layers atop a silicon substrate that were then readily cross-linked into insoluble solid-state films by UV irradiation. As a proof of concept, three such layers were constructed atop one another and imaged with scanning electron microscopy (SEM). The cross section in Figure 5e depicts a thick hybrid film where individual layers may be resolved.

Table 1. Heat storage and release properties of the azobenzene-based monomer and polymer.

Property	Monomer	Polymer
Energy density [Wh kg^{-1}]	42 ± 2	29 ± 2
Half-life [h]	92 ± 1	55 ± 1
Cycling stability [no. of cycles]	>100	>100

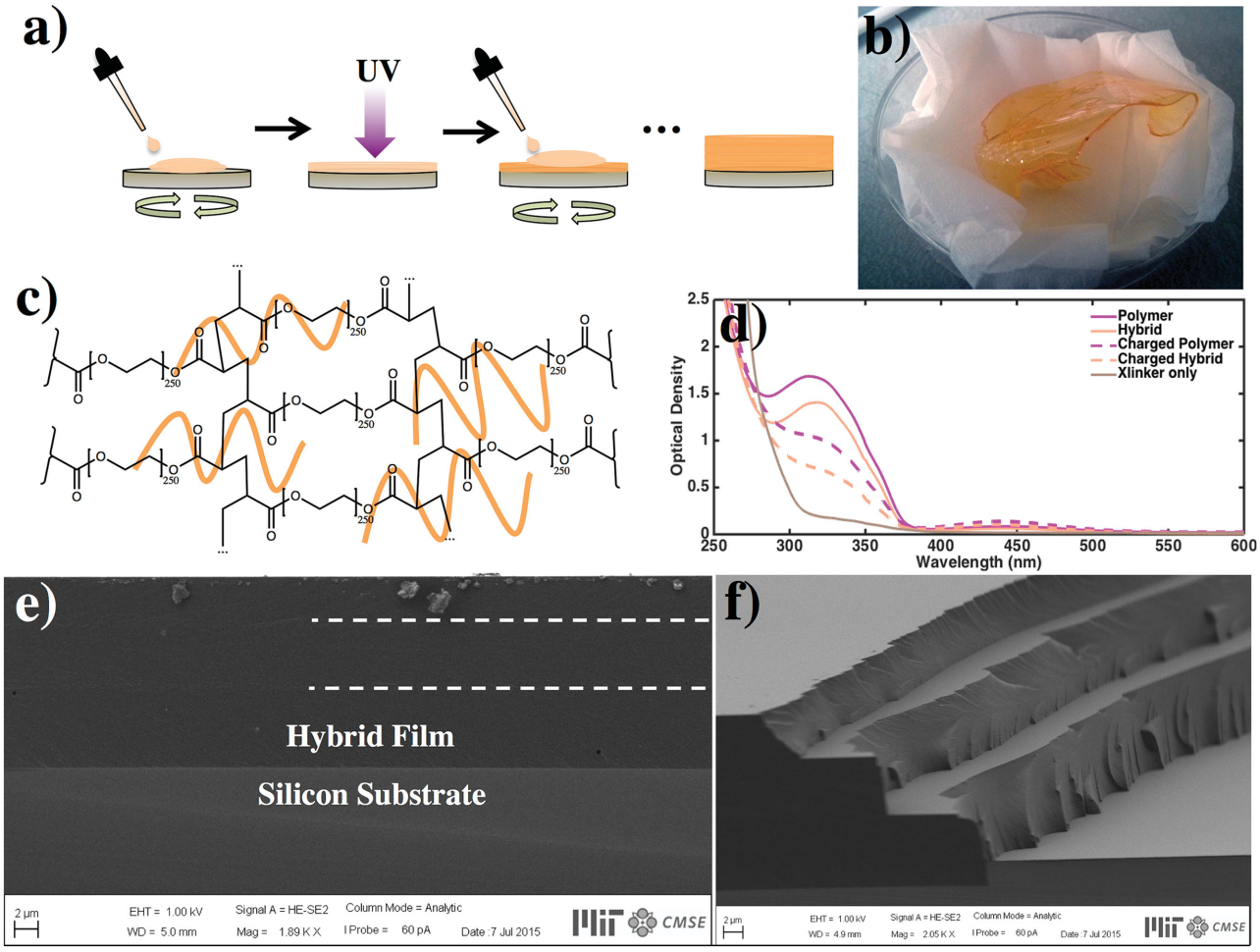

Figure 5. Cross-linking approach for layer-by-layer solid-state STFs. a) Cross-linking concept of the STF polymer film employing a hybrid solution of STF and cross-linker. UV curing results in an insoluble layer allowing new layers to be deposited on top. b) Photograph of a freestanding, large area polymer STF film generated using the cross-linking approach. c) Molecular concept for the incorporation of the polymer STF into a cross-linked poly(ethylene glycol) diacrylate matrix. d) Charging properties of the polymer and hybrid films, as well as optical properties of cross-linked poly(ethylene glycol) diacrylate. e) Cross-sectional SEM image of three layer-by-layer hybrid films where individual layers may be resolved (dashed lines), exhibiting exceptional uniformity and adhesion between layers. f) Sheared hybrid film from (e) where three layers may be clearly resolved atop one another.

To better resolve the three layers, the film was intentionally sheared to reveal the profile shown in Figure 5f. Importantly, these films are very uniform, adherent to one another, and present a scalable way to make variable thickness STECs not limited by the spin-coating approach. This engineering concept presents further opportunities to incorporate cross-linking units onto the azobenzenes themselves in order to increase STF loading or to construct co-polymers with cross-linkable moieties,[38,39] where the ratio of STF to cross-links may be precisely controlled.

Though the charging, discharging, and appreciable energy release have been demonstrated for our STF polymer materials, it still remains to determine their efficacy as macroscale heat-release STECs for realistic solid-state applications. Within the STEC platform, the substrate mass is ≈1.8 g, with a heat capacity of 0.8 J g^{-1}, effectively requiring ≈100 mg of polymer STF to show any appreciable temperature change upon heat release (5–10 °C). However, given the mass required and thickness scaling from Figure 3f,g (approximately linear with mass), a thickness on the order of 50–100 µm is desirable. Given the considerations in Figure 4c, such a film would require increased charging requirements. Hence, in order to ensure complete charging and demonstrate macroscopic heat release, we instead rapidly charge our materials at a low concentration (≈1 mg mL^{-1}) in the solution state, where charging and deposition solvents need to be chosen judiciously to maximize the energy density (Experimental Section). Then, we develop a multistage drop casting method in order to build up a thick film, though with greater morphological variation than our spin-coated STECs. In order to measure the heat release, we design an experimental setup that triggers the reverse thermal isomerization using a heating stage (**Figure 6**a), while simultaneously measuring the spatial temperature profile with an infrared camera (Video S1, Supporting Information). The response shown in Figure 6b from the uncharged and charged films is vastly different, where after initial stabilization such that the temperature difference between the two films is constant, the charged film temperature sharply overtakes the

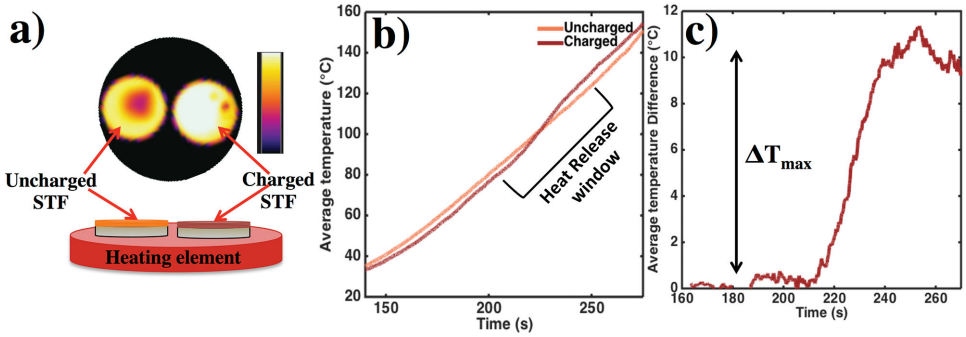

Figure 6. Macroscopic STF polymer heat release. a) Top-view IR heat map of uncharged and charged solar thermal energy capacitors (STECs) placed on a heating element, with side-view illustration below. Heat map depicted for maximal temperature difference between samples with color bar indicating relative heat magnitude. b) Average temperature recorded on the surface of each STEC plotted as a function of experiment time. c) Average temperature differences between the two STECs after normalization at the stabilization temperature ≈160 s into the experiment, at least a 10 °C total change (ΔT_{max}) in temperature is observed between the samples due to heat release by the charged STF polymer.

control film at ≈100–110 °C, consistent with independent DSC measurements. Given the scale of the experiment, thermal coupling within the system, and some inhomogeneity between the STECs, the temperature variation was as high as 2–3 °C for control trials on several uncharged films (Section S4, Supporting Information), indicating that the measured result was well above this temperature variation. To gain a better appreciation for the temperature release, in Figure 6c we normalize the curve at the point where they have both reached a constant temperature difference (≈160 s, 40 °C in Figure 6b) and plot the temperature difference. A dramatic temperature spike at 220 s results in a ≈10 °C average temperature difference between the charged and uncharged STECs. Importantly, this heat release results in a temperature difference on the order of several tens of seconds, which is important for certain rapid heat-release applications, and serves as the first demonstration of macroscopic, solid-state application-oriented heat release from an STF material.

3. Conclusion

The development of the solar thermal fuel capacitor platform using polymer films has enabled the charging, discharging, and heat release using optically chargeable molecules within the solid-state. Polymer STF materials enable uniform morphologies that can span thicknesses of 100 nm to several tens of micrometers with added tunability by employing UV-activated cross-links. By studying the charging and discharging properties, and the heat energy stored within the STECs, it was possible to construct a macroscopic device resulting in temperature differences as high as 10 °C, demonstrating the feasibility of these devices for solid-state applications. Given the rich chemistry available on the monomer and the polymer backbone, future approaches can leverage these additional degrees of freedom to enhance the energy density, improve the optical chargeability and photostationary state, and collect photons across a greater portion of the solar spectrum. With such unprecedented materials flexibility and demonstrated feasibility for solid-state applications, STF materials employed in the solid-state present a tremendously attractive avenue for both fundamental light-matter interaction science and novel solid-state applications for renewable energy storage and heat release.

Experimental Section

Density Functional Theory: We carried out standard ab initio calculations within the DFT framework, using the Vienna Ab Initio Simulation Package (VASP, v5.3). Plane wave and projector-augmented wave (PAW) type pseudopotentials with kinetic-energy cutoffs of up to 400 eV were employed, along with the Perdew-Burke-Ernzerhof exchange-correlation functional.

Monomer Synthesis: The monomer was synthesized based on a published recipe.[40] Briefly, phenylazophenol (2 g) was dissolved in tetrahydrofuran (THF, 25 mL) and triethylamine (1.4 mL) in anhydrous and oxygen free conditions. Methacryloyl (3 mL) chloride was added dropwise under inert conditions, while cooling reaction in an ice bath (resulting in gas evolution, dark color change, and salt precipitate). The reaction was left stirring at room temperature for 48 h. Extraction was done by diluting four times with 3:1 mix of dichloromethane (DCM) (or chloroform) and water. The organic phase was dried with sodium sulfate and dried under vacuum (<0.1 mbar) overnight. The resultant material was purified in a silica column using 1:1 DCM:hexanes. Overall reaction yield was between 70% and 80%.

Polymer Synthesis: In a typical homopolymerization, the monomer (0.1 g) was dissolved in anhydrous THF (1 mL) and azobisisobutyronitrile (AIBN, 3 mg) was added. The solution was subjected to three freeze/pump/thaw cycles. The reaction was run under inert conditions at 65 °C for 3 h. The polymer was isolated in a solution of stirred methanol and then filtered and rinsed with additional methanol. The reaction is easily scaled to 1 g. Maximum yields obtained were 80%.

Size Exclusion Chromatography: SEC measurements were performed on 0.5 mg mL^{-1} samples in stabilized, High Performance Liquid Chromatography (HPLC)-grade tetrahydrofuran using an Agilent 1260 Infinity system with variable-wavelength diode array (254, 450, and 530 nm) and refractive index detectors, guard column (Agilent PLgel; 5 µm; 50 mm × 7.5 mm), and three analytical columns (Agilent PLgel; 5 µm; 300 mm × 7.5 mm; 105, 104, and 103 Å pore sizes). The instrument was calibrated with narrow-dispersity polystyrene standards between 1.7 and 3150 kg mol^{-1}. All runs were performed at 1.0 mL min^{-1} flow rate and 35 °C. Molecular weight values were calculated using Chemstation Gel Permeation Chromatography Data Analysis Software (Rev. B.01.01) based on the refractive index signal.

UV–Vis Measurements: Absorption was carried out using a Cary 5000, with 100 µm concentrations in a 10 cm path length quartz cuvette.

Solid-state measurements were carried out on 1 in. circular quartz substrates. Charging in situ was done using a high-power UV lamp, while cycling was done by optical charging and discharging using an arc lamp and filters to excite the $\pi > \pi^*$ and $n > \pi^*$ transitions of the *trans* and *cis* isomers, respectively.

Image Acquisition: Film photographs were obtained using a conventional optical microscope. High magnification images and cross-sections were obtained using a Zeiss Merlin scanning electron microscope by depositing materials on a single crystal silicon substrate.

Solid-State Film Preparation: Spin coating was carried out at 1000 rpm on 1 in. quartz substrates. Films were dried overnight in air ambient conditions. Cross-linked films were made by dissolving the polymer in poly(ethylene glycol) diacrylate (n = 250) under inert conditions and using a 2,2-dimethoxy-2-phenylacetophenone photoinitiator. A UV lamp (3 W) was used to cross-link the film. Thickness measurements were obtained using a DekTak 6.

Charging and *Differential Scanning Calorimetry*: Solution samples in toluene were charged using a 365 nm 100 W UV lamp while cooled at 25 °C while stirring. Solid-state samples were kept at 30 °C using a cooling stage while charged using the 100 W lamp at a distance of 10 cm. Films were subsequently redissolved in DCM or toluene (solvent had no impact on DSC energy density values). The solutions were dried in DSC pans in the dark and sealed, giving a final mass of 1 mg of material. DSC was carried out using a TA Instruments DSC Q20.

Macroscopic Heat Release: The polymer (100 mg) was charged in a large flask while being cooled to 10 °C first in toluene for 16 h and then transferred to acetone and charged overnight. The charged material was dried using vacuum to a volume of 1 mL and then drop cast in several steps with a 30 min vacuuming step in between. A final vacuum (1 mbar) was applied for 6 h before discharge. Discharging was done relative to an uncharged control on a hot plate while monitoring with an infrared camera (FLIR Ax5).

Supporting Information

Supporting Information is available from the Wiley Online Library or from the author.

Acknowledgements

D.Z. acknowledges his Natural Sciences and Engineering Research Council of Canada Banting Fellowship. Materials and resources funding for this project was provided by Bavarian Motor Works (BMW). The authors thank Dr. Torsten Frank (BMW) for helpful discussions.

Received: October 8, 2015
Revised: November 20, 2015
Published online:

[1] T. J. Kucharski, Y. Tian, S. Akbulatov, R. Boulatov, *Energy Environ. Sci.* **2011**, *4*, 4449.
[2] A. Lennartson, A. Roffey, K. Moth-Poulsen, *Tetrahedron Lett.* **2015**, *56*, 1457.
[3] V. Gray, A. Lennartson, P. Ratanalert, K. Borjesson, K. Moth-Poulsen, *Chem. Commun.* **2014**, *50*, 5330.
[4] V. A. Bren', A. D. Dubonosov, V. I. Minkin, V. A. Chernoivanov, *Russ. Chem. Rev.* **1991**, *60*, 451.
[5] R. Boese, J. K. Cammack, A. J. Matzger, K. Pflug, W. B. Tolman, K. P. C. Vollhardt, T. W. Weidman, *J. Am. Chem. Soc.* **1997**, *119*, 6757.
[6] K. Börjesson, D. Ćoso, V. Gray, J. C. Grossman, J. Guan, C. B. Harris, N. Hertkorn, Z. Hou, Y. Kanai, D. Lee, J. P. Lomont, A. Majumdar, S. K. Meier, K. Moth-Poulsen, R. L. Myrabo, S. C. Nguyen, R. A. Segalman, V. Srinivasan, W. B. Tolman, N. Vinokurov, K. P. C. Vollhardt, T. W. Weidman, *Chem. Eur. J.* **2014**, *20*, 15587.
[7] Y. Kanai, V. Srinivasan, S. K. Meier, K. P. C. Vollhardt, J. C. Grossman, *Angew. Chem. Int. Ed.* **2010**, *49*, 8926.
[8] A. W. Adamson, A. Vogler, H. Kunkely, R. Wachter, *J. Am. Chem. Soc.* **1978**, *100*, 1298.
[9] R. J. Corruccini, E. C. Gilbert, *J. Am. Chem. Soc.* **1939**, *61*, 2925.
[10] T. J. Kucharski, N. Ferralis, A. M. Kolpak, J. O. Zheng, D. G. Nocera, J. C. Grossman, *Nat. Chem.* **2014**, *6*, 441.
[11] K. Masutani, M. Morikawa, N. Kimizuka, *Chem. Commun.* **2014**, *50*, 15803.
[12] Y. Liu, J. C. Grossman, *Nano Lett.* **2014**, *14*, 7046.
[13] K. Ishiba, M. Morikawa, C. Chikara, T. Yamada, K. Iwase, M. Kawakita, N. Kimizuka, *Angew. Chem. Int. Ed.* **2015**, *54*, 1532.
[14] W. Luo, Y. Feng, C. Cao, M. Li, E. Liu, S. Li, C. Qin, W. Hu, W. Feng, *J. Mater. Chem. A* **2015**, *3*, 11787.
[15] T. A. Singleton, K. S. Ramsay, M. M. Barsan, I. S. Butler, C. J. Barrett, *J. Phys. Chem. B* **2012**, *116*, 9860.
[16] X. Cheng, Q. Li, C. Li, J. Qin, Z. Li, *Chem. – Eur. J.* **2011**, *17*, 7276.
[17] G. K. Joshi, K. N. Blodgett, B. B. Muhoberac, M. A. Johnson, K. A. Smith, R. Sardar, *Nano Lett.* **2014**, *14*, 532.
[18] V. Ferri, M. Elbing, G. Pace, M. D. Dickey, M. Zharnikov, P. Samorì, M. Mayor, M. A. Rampi, *Angew. Chem.* **2008**, *120*, 3455.
[19] G. Haberhauer, C. Kallweit, *Angew. Chem. Int. Ed.* **2010**, *49*, 2418.
[20] T. Ube, T. Ikeda, *Angew. Chem. Int. Ed.* **2014**, *53*, 10290.
[21] S. Kobatake, S. Takami, H. Muto, T. Ishikawa, M. Irie, *Nature* **2007**, *446*, 778.
[22] D. H. Wang, J. J. Wie, K. M. Lee, T. J. White, L.-S. Tan, *Macromolecules* **2014**, *47*, 659.
[23] C. Weber, T. Liebig, M. Gensler, L. Pithan, S. Bommel, D. Bléger, J. P. Rabe, S. Hecht, S. Kowarik, *Macromolecules* **2015**, *48*, 1531.
[24] S. Fu, Y. Zhao, *Macromolecules* **2015**, *48*, 5088.
[25] M. Petr, P. T. Hammond, *Macromolecules* **2011**, *44*, 8880.
[26] Z. Li, Y. Zhang, L. Zhu, T. Shen, H. Zhang, *Polym. Chem.* **2010**, *1*, 1501.
[27] A. A. Beharry, O. Sadovski, G. A. Woolley, *J. Am. Chem. Soc.* **2011**, *133*, 19684.
[28] T. P. Osedach, T. L. Andrew, V. Bulovic, *Energy Environ. Sci.* **2013**, *6*, 711.
[29] H. Rau, *Photoisomerization of Azobenzenes*, Vol. *2*, CRC Press, Boca Raton, FL **1990**.
[30] J. Garcia-Amoros, A. Sanchez-Ferrer, W. A. Massad, S. Nonell, D. Velasco, *Phys. Chem. Chem. Phys.* **2010**, *12*, 13238.
[31] J. García-Amorós, D. Velasco, *Beilstein J. Org. Chem.* **2012**, *8*, 1003.
[32] H. M. D. Bandara, S. C. Burdette, *Chem. Soc. Rev.* **2012**, *41*, 1809.
[33] Y.-Q. Shen, H. Rau, *Makromol. Chem.* **1991**, *192*, 945.
[34] M. Schönhoff, M. Mertesdorf, M. Lösche, *J. Phys. Chem.* **1996**, *100*, 7558.
[35] H. Chen, T. N. Cong, W. Yang, C. Tan, Y. Li, Y. Ding, *Prog. Nat. Sci.* **2009**, *19*, 291.
[36] M. Tsuda, K. Kuratani, *Bull. Chem. Soc. Jpn.* **1964**, *37*, 1284.
[37] A. M. Kolpak, J. C. Grossman, *J. Chem. Phys.* **2013**, *138*, 034303.
[38] G. Han, H. Zhang, J. Chen, Q. Sun, Y. Zhang, H. Zhang, *New J. Chem.* **2015**, *39*, 1410.
[39] C. Qin, Y. Feng, W. Luo, C. Cao, W. Hu, W. Feng, *J. Mater. Chem. A* **2015**, *3*, 16453.
[40] M. Moniruzzaman, C. J. Sabey, G. F. Fernando, *Macromolecules* **2004**, *37*, 2572.